CONFIDENTIAL

Copy
RM L54B17a

NACA RM L54B17a

NACA

RESEARCH MEMORANDUM

A WIND-TUNNEL INVESTIGATION OF THE FIRST-ORDER VIBRATORY STRESSES ON A FULL-SCALE SUPERSONIC-TYPE PROPELLER OPERATING IN AN ASYMMETRIC AIR FLOW

By Atwood R. Heath, Jr., and Robert L. O'Neal

Langley Aeronautical Laboratory
Langley Field, Va.

NATIONAL ADVISORY COMMITTEE
FOR AERONAUTICS

WASHINGTON

November 2, 1954

CONFIDENTIAL

NATIONAL ADVISORY COMMITTEE FOR AERONAUTICS

RESEARCH MEMORANDUM

A WIND-TUNNEL INVESTIGATION OF THE FIRST-ORDER VIBRATORY STRESSES ON A FULL-SCALE SUPERSONIC-TYPE PROPELLER OPERATING IN AN ASYMMETRIC AIR FLOW

By Atwood R. Heath, Jr., and Robert L. O'Neal

SUMMARY

An investigation of the first-order, 1xP, vibratory-stress characteristics of a three-blade supersonic-type propeller of 12-foot diameter operating in an asymmetric air flow has been made on the NACA 6,000-horsepower propeller dynamometer in the Langley 16-foot transonic tunnel. The investigation covered a blade-angle range from 19.7° to 46.3°, a rotational-speed range from 1,300 to 2,100 rpm, and a forward Mach number range from 0.20 to 0.94.

The results indicate that the measured radial location of the maximum first-order vibratory stress and the measured apparent first-order resonant frequency agree well with calculations.

Analytical consideration of the maximum first-order resonant stress, to evaluate the allowable flight conditions for a hypothetical airplane, indicates that maneuvering load factors as large as 5 may be negotiated at sea level and as large as 3 at 20,000-foot altitude without exceeding a bending stress of ±30,000 lb/sq in. (for flight Mach number of 0.94).

INTRODUCTION

Propeller blades designed to operate at high-subsonic and low-supersonic forward speeds must of necessity have thin airfoil sections extending well inboard in order to obtain optimum aerodynamic efficiency. The use of thin airfoil sections, however, may result in a flexible blade structure with a low fundamental bending frequency. If a once-per-revolution excitation, 1xP, such as that caused by thrust-axis inclination, is present and the fundamental bending frequency falls within the

operating range, a resonant condition will occur. Since the magnitude of the vibratory stress at resonance is dependent in large measure on the propeller-blade aerodynamic damping, about which little is known, critically high stresses even at small angles of inclination may result.

Consequently, a full-scale supersonic-type propeller of 12-foot diameter, the Aeroproducts A39SFN-161A three-blade propeller, for which the predicted fundamental bending frequency fell within the operating range has been investigated in the Langley 16-foot transonic tunnel in order to determine the first-order resonant frequency as well as the magnitude of the vibratory stresses encountered at resonance. The propeller was operated under a once-per-revolution excitation over a blade-angle range at the 0.75-radius station from 19.7° to 46.3°, a rotational-speed range from 1,300 to 2,100 rpm, and a forward Mach number range from 0.20 to 0.94.

SYMBOLS

A	angle of thrust axis with respect to airstream (inflow angle), deg
A_e	effective airstream angle (apparent inflow angle), deg
b	blade width (chord), ft
C_T	thrust coefficient, $\frac{T}{\rho n^2 D^4}$
c/c_c	ratio of damping to critical damping (see ref. 7)
D	propeller diameter, ft
h	blade-section maximum thickness, ft
M	Mach number of advance
M.F.	vibratory-stress magnification factor
N	propeller rotational speed, rpm
n	propeller rotational speed, rps
q	free-stream dynamic pressure, $\frac{1}{2}\rho V^2$, lb/sq ft
q_e	free-stream dynamic pressure for conditions associated with A_e

R	propeller tip radius, ft
r	radius to blade element, ft
T	thrust, lb
V	velocity of advance, ft/sec
x	fraction of propeller tip radius, r/R
β	blade angle, deg
ρ	mass density of air, slugs/cu ft
σ	vibratory stress, lb/sq in
ω_n	undamped fundamental natural bending frequency, cpm

APPARATUS

The Langley 16-Foot Transonic Tunnel

The investigation was conducted in the Langley 16-foot transonic tunnel which has a slotted test section. Reference 1 gives the Mach number distributions in the test section as found by the tunnel calibration with the NACA 6,000-horsepower propeller dynamometer installed with no propeller.

The NACA 6,000-Horsepower Propeller Dynamometer

The two units of the NACA 6,000-horsepower propeller dynamometer were coupled in tandem with the propeller mounted on the forward end as shown in figure 1. For setting thrust and torque of the propeller, pressure gages that convert the pneumatic pressures of the thrust and torque capsules to direct readings were used. A complete description of the dynamometer is given in reference 2. A cylindrical body of the same diameter as the dynamometer case extended forward from the propeller to the downstream end of the tunnel-entrance cone, and was supported by three struts located radially around the body and well forward of the propeller. There was no spinner available for the propeller so the cylindrical body and the dynamometer case were abruptly tapered to the propeller hub. A sketch of the dynamometer and cylindrical body mounted in the tunnel test section is shown in figure 2.

Test Propeller

A three-blade propeller, 12 feet in diameter, having the Aeroproducts designation A39SFN-161A was used for the investigation. The propeller was designed to operate at a rotational speed of 2,100 rpm and a forward Mach number of 0.95 at a 40,000-foot altitude which represents an advance ratio of 2.2. The blades (separately designated as Aeroproducts A91A1-144-0) were made of solid SAE 4130 steel and had symmetrical NACA 16-series airfoil sections. The blades tapered from a chord of 20 inches at the 0.21-radius station to 14 inches at the tip, and the thickness ratio varied from 0.09 at the 0.21-radius station to 0.02 at the tip. The bladeform curves and developed plan form are shown in figure 3. The propeller hub was of a three-way, controllable-pitch type, but for these tests was used as a fixed-pitch, ground-adjustable hub.

Reference Propeller

For determining the effective airstream angularity, the NACA 10-(3)(08)-03 three-blade propeller was used. Complete details of this propeller are given in reference 3 and the manner in which the propeller was used is given in the appendix of the present paper.

Wake-Survey Rakes

The wake-survey rake struts were of circular-arc cross section having a chord of 2 feet and a thickness ratio of 0.08. The leading edge of each rake strut was located 44 inches behind the plane of the propeller and the pressure orifices were located 2 feet ahead of the leading edge of the strut. The rake configuration used showing rake angular locations is shown in figure 4, and a view of the rakes may be seen in figure 1.

Instrumentation

Propeller-blade vibratory stresses were measured by using phenolic-bonded-type wire strain gages mounted at the 0.50 chord on the upper surface of the gaged blade. Gages were mounted to read both vibratory bending and vibratory torsional stresses. The gage locations are shown in figure 5 on a projected blade plan form. Electrical output from the strain gages was transmitted through a slipring device and amplifiers to a recording oscillograph and was recorded on photographic paper. A proportionality factor of stress to photographic trace deflection was obtained at the beginning and end of each run, thereby making the conversion of the vibratory record to stress a simple process.

GENERAL CONSIDERATIONS

Propeller investigations in the Langley 16-foot transonic tunnel prior to the present investigation revealed the presence of a once-per-revolution 1xP excitation although the propeller thrust axis was alined with the tunnel center line (see ref. 1). It was found that the magnitude of the excitation varied with survey-rake angular position. Consequently, the nature of the excitation could not be determined by a complete survey behind the propeller disk.

Three possible asymmetric flow conditions that could cause the propeller to react as though it were subject to thrust-axis inclination, all of which were probably present to some extent, are as follows:

(1) Misalinement of the airstream with the tunnel center line.

(2) Local airstream angularities

(3) Local airstream velocity variations

The effective airstream angle may then be defined as an equivalent propeller thrust-axis inclination angle that would give the same resultant 1xP vibratory aerodynamic loads and vibratory blade stresses as those caused by the asymmetric flow.

Tilting the propeller thrust axis to obtain a known inflow was not attempted as it was expected that any change in the dynamometer configuration would have affected the 1xP excitation by an undetermined amount, thus invalidating the results.

The method used for obtaining the effective airstream angle was to measure the 1xP stress on an operating propeller in the dynamometer and wind-tunnel configuration of this investigation and to relate these stresses to stresses which had been obtained on the same propeller when operated under known inflow conditions.

TESTS

Tests were conducted at blade angles of 19.7°, 29.3°, 39.1°, and 46.3° measured at the 0.75-radius station. All blade-angle tests were conducted over a propeller rotational-speed range from 1,300 to 2,100 rpm except for the two higher blade-angle runs which were limited by excessive dynamometer vibration and blade vibratory stresses. At each blade angle and rotational speed, the tunnel Mach number was set to give approximately zero propeller thrust which for the complete investigation represented an overall Mach number range from 0.20 to 0.94.

Tests to determine the effective airstream angularity by using the NACA 10-(3)(08)-03 three-blade propeller included a rotational-speed range from 1,300 to 2,000 rpm. The blade angles tested were 20°, 30°, 40°, 50°, and 55° measured at the 0.75-radius station. The tunnel Mach number was set to give approximately zero propeller thrust at each test point, which gave an overall Mach number range from 0.21 to 0.90 for the complete investigations.

REDUCTION OF DATA

Tunnel Velocity

The tunnel velocity in the plane of the propeller was obtained from the tunnel calibration made for the investigation of reference 1, with the dynamometer installed with no propeller.

Vibratory Stress

The 1xP excitation was of an extremely erratic nature and showed a variation of amplitude with time. For some stress records, the variation in amplitude was of the order of 45 percent of the maximum amplitude. Figure 6 shows a typical oscillograph record in which a variation of about 20 percent in the magnitude of the vibratory stress with time is shown. The vibratory stress was read at a point on each record where the maximum stress remained constant for several cycles. Although the stress appeared to be predominately 1xP, each record was analyzed by means of a 12-point Fourier series to determine the 1xP component, which is presented as the 1xP vibratory stress.

Because of the large variation in vibratory stress with time, the possibility exists that the maximum stress for any given test point may not have been recorded; however, the analyzed data when presented as a function of propeller rotational speed generally show less than a 10 percent scatter from a faired curve.

Effective Airstream Angle

The method for reducing the data to obtain the effective airstream angle is given in the appendix. Because of the variation of the 1xP excitation, as well as the other assumptions made in determining the effective airstream angle, it is considered to be accurate only within 0.50°.

RESULTS AND DISCUSSION

The representative first-order 1xP vibratory bending stresses are presented in figures 7 and 8. No 1xP vibratory stresses in the torsional mode of vibration were noted on the stress records.

Figure 7 shows the radial distribution of the 1xP vibratory bending stresses for the top rotational speed reached at each propeller blade angle. The maximum-bending-stress location was at or very close to the $x = 0.243$ strain-gage location which was in the transition region where the blade was rapidly becoming thicker toward the root, as seen in figure 3. The location of the maximum bending stress was in good agreement with the calculations of reference 4 in which the bending moments when expressed as stresses were found to indicate the same maximum stress location.

Figure 8 presents the variation of the 1xP vibratory bending stress, measured at the maximum stress location of $x = 0.243$, with propeller rotational speed for the various blade angles investigated. Figure 9, which shows the variation of forward Mach number and dynamic pressure with propeller rotational speed for all test conditions, is presented so that additional calculations may be made if so desired. The effective airstream angles that are considered to be applicable to the propeller are shown in figure 10 as a function of dynamic pressure for the various rotational speeds.

For each blade angle shown in figure 8, the 1xP bending stress increased with rotational speed for the following reasons:

(1) The effective airstream angle A_e increased with rotational speed and caused the excitation parameter $A_e q_e$ to become larger. The 1xP vibratory stress has been shown to increase with Aq in reference 3.

(2) The dynamic pressure q_e also increased because the tunnel airspeed was increased along with rotational speed in order to keep the thrust near zero, thus making the excitation factor greater.

(3) The approach to blade resonance caused a greater magnification of the 1xP stresses.

The 1xP stress did not increase as did $A_e q_e$ for the two lowest blade angles of figure 8, the increase in stress being less than would be expected from an inspection of the $A_e q_e$ values. This result was attributed to the inaccuracies in stress determination that prevailed for small values of vibratory stress.

The rapid increase in slope of the vibratory-bending-stress curve beyond 1,800 rpm for the $\beta_{0.75R} = 46.3^\circ$ curve of figure 8 was typical of a one-degree-of-freedom response curve of low damping near resonance. Although phase angles between the applied loads and the resulting stresses could not be determined, the phase angles between the stresses and an arbitrary propeller angular location were obtained. Large scatter was noted for the three lowest blade-angle tests but the phase angles appeared essentially to be constant with rotational speed. However, for the $\beta_{0.75R} = 46.3^\circ$ test, an increase in phase angle of about 90° was noted over the rotational-speed range, further indicating that resonance was imminent. Therefore, it was assumed that the highest propeller rotational speed reached, 2,025 rpm, was at 1xP resonance or slightly below a resonant condition. Positive identification of resonance could not be made as the total vibratory stress had reached the limit of safe operation for this investigation. Figure 11 gives the comparison of the measured apparent resonant point with resonant conditions calculated in references 4 and 5. The agreement of the measured point with the calculated curve of reference 5, which utilized the Rayleigh-Ritz method involving four independent coordinates, was very good. In reference 4, the propeller of this investigation was designated A39SFN-125 and in reference 5 it was designated A. F. blade.

Since the propeller appeared to be operating at or very near resonance at a blade angle of $\beta_{0.75R} = 46.3^\circ$ and a rotational speed of 2,025 rpm, it is seen from the magnification factor equation, which is given in the appendix, that the magnification of the 1xP vibratory stress depended only on the damping in the system. It has been shown in reference 3 that the 1xP stress increased linearly with Aq for a given rotational speed. However, if the propeller was operating at 1xP resonance at a constant blade angle, the 1xP stress would be linear with Aq only if the damping of the system remained a constant. An example of the effect of aerodynamic damping on the 1xP stress is indicated in figure 12. The relation of air density and propeller resultant velocity to damping force as presented in reference 6 was applied to the magnification factor for the apparent resonant stress of figure 8. The variation of 1xP stress with altitude (or density) was obtained for $A_e q_e = 1{,}490$ at the same blade angle, rotational speed, and forward Mach number as the apparent resonant point. The $A_e q_e$ value of 1,490 was determined from figure 9 and an extrapolation of the 2,000-rpm curve of figure 10. The family of curves of constant Aq was based on the linear relationship of 1xP stress with Aq. The trend of the 1xP stress with altitude for a given Aq indicates that operation at sea level results in the lowest vibratory stresses. For example, if the propeller operating conditions which gave the data point of figure 12 were altered only by operation at sea level instead of at the density altitude of 13,300 ft, the 1xP stress would be reduced by about 35 percent. The increase in damping was due to the increase in air density at the lower altitude. Curves of constant thrust-axis inclination

angle have also been included (see fig. 12) which correspond to operation at a decreasing Δq with increase in altitude.

By keeping Mach number a constant in the analysis of the 1xP stress changes with altitude there would be a decrease in the forward velocity with increasing altitude which would result in an increased loading on the propeller. Since no resonant 1xP stress measurements were made at positive propeller loadings, the 1xP stress at zero thrust has been assumed to apply for the altitude range which corresponds to rather wide changes in thrust loading. Such an assumption might make the stresses at the higher altitudes unconservative since the data of reference 3, which were obtained on a much more rigid propeller, indicated that for the same Δq an increase of thrust from zero to thrust at peak efficiency caused a 21 percent increase in stress. However, although the curves of figure 12 do not show an actual operating regime for the propeller, the effect of aerodynamic damping is nevertheless demonstrated. Direct comparison of the measured apparent resonant stress with stress adjusted to sea-level operation is valid since the forward velocities and, hence, propeller thrust coefficient were the same for both conditions.

The operating field represented by figure 12 with inflow angles to 3° and altitudes to 20,000 feet indicates the maximum 1xP stresses that would be anticipated for the propeller of this investigation installed on an airplane flying at $M = 0.94$ having a wing loading of 60 lb/sq ft, and maneuvering at normal load factors as high as 5 at sea level and 3 at 20,000 feet. The analysis was made by assuming that the propeller thrust axis was alined with the airplane axis and that any upwash to the wing or fuselage was sufficiently small to cause no effect on the inflow angle to the propeller plane. However, higher airplane attitudes may be obtained by tilting the thrust axis downward. For operation-off resonance, the relatively large 1xP stresses shown in figure 12 would not be expected for the given Δq values; hence, higher values of Δq would be acceptable for airplane operation. For example, take-off where a lower blade-angle setting would be used corresponds to an off-resonant condition.

CONCLUDING REMARKS

From the present investigation and from analytical application of the data to a hypothetical airplane, the following remarks can be made concerning the first-order vibratory characteristics of a full-scale supersonic-type three-blade propeller.

The measured radial location of the maximum first-order vibratory stress and the measured apparent first-order resonant frequency agree well with calculations.

Analytical consideration of the maximum measured first-order resonant stress, to evaluate the allowable flight conditions for a hypothetical airplane, indicates that maneuvering load factors as large as 5 may be negotiated at sea level and as large as 3 at 20,000-foot altitude without exceeding a bending stress of ±30,000 lb/sq in. (for a flight Mach number of 0.94).

Langley Aeronautical Laboratory,
National Advisory Committee for Aeronautics,
Langley Field, Va., February 9, 1954.

APPENDIX

A METHOD FOR DETERMINING THE EFFECTIVE AIRSTREAM ANGULARITY

The method used for obtaining the effective airstream angle was to measure the 1xP stresses on an operating propeller in the dynamometer and wind-tunnel configuration of this investigation and to relate these stresses to stresses which had been obtained on the same propeller when operated under known inflow conditions. The NACA 10-(3)(08)-03 three-blade propeller had been investigated under known inflow conditions and the results were presented in reference 3. Figure 13 shows analyzed 1xP stress data at approximately zero thrust that were published in reference 3 as unanalyzed data, and the linearity of the stress with Δq may be noted. Separate curves had been obtained for the different rotational speeds which, as was explained in reference 3, were accounted for by differences in aerodynamic excitation as well as propeller-blade dynamic effects. If the same propeller was operated at the same condition but at an unknown excitation as in the present case, a 1xP stress for the same radial location was obtained at a known dynamic pressure. The 1xP stress value at the unknown excitation from the present tests was used to obtain Δq from figure 13 and the effective airstream angle was determined as follows:

$$A_e = \frac{\Delta q}{q_e}$$

Tests at blade angles other than $\beta_{0.75R} = 30^\circ$ were necessary in order to cover the Mach number range of the present investigation. The 1xP stresses obtained at blade angles other than $\beta_{0.75R} = 30^\circ$ could not be used directly with figure 13 to obtain the effective airstream angles because of the variation in stress magnification factors caused by the change in fundamental natural bending frequency of the rotating blade with blade angle. The magnification factors for the stresses obtained at each blade angle and rotational speed were, therefore, first calculated by means of the one-degree-of-freedom equation of reference 7 in which a slightly different notation is used.

$$\text{M.F.} = \frac{1}{\sqrt{\left(1 - \frac{N^2}{\omega_n^2}\right)^2 + \left(2\frac{c}{c_c}\frac{N}{\omega_n}\right)^2}}$$

The fundamental natural bending frequency of the rotating blade ω_n was then obtained from figure 14 which has been calculated by the Propeller Laboratory of Wright Air Development Center by using the method of reference 5. The ratio of damping to critical damping c/c_c has been determined in reference 8 for a propeller similar to the NACA 10-(3)(08)-03 and was found to be approximately 0.03. Since the calibration propeller was not operated in the immediate vicinity of resonance, small changes in damping would have a negligible effect on the magnification factors. In order to determine values of A_e from figure 13 at blade angles other than 30°, the 1xP stresses measured at these angles were normalized to correspond to the 30° condition by taking the difference of amplification factors into account.

The results of the calibration tests are shown in figure 10 which gives the variation of A_e with dynamic pressure for all operating conditions of the calibration propeller, and the faired curves are considered to be representative of the effective airstream angles affecting the A39SFN-161A propeller when operating at the same rotational speeds. In determining A_e and considering its applicability to the A39SFN-161A propeller, two assumptions have been made. First, the difference in the diameters of the two propellers would have a negligible effect on the asymmetric flow conditions causing the 1xP excitation. No evaluation of this effect could be made but it was assumed to be small. Second, in considering the calibration propeller for blade angles other than $\beta_{0.75R} = 30°$, it was assumed that the effects of resultant blade-section Mach numbers on the vibratory forcing function were accounted for solely by relating the data to the previously obtained data of reference 3 at the same rotational speeds. The latter effect has been investigated insofar as possible and the only method of evaluation available was by comparison of wake-survey distributions. Radical changes in the wake-survey distributions due to section Mach number increases were noted for two conditions. The conditions which were 2,000 rpm at $\beta_{0.75R} = 50°$ and 1,600 rpm at $\beta_{0.75R} = 55°$ have not been included in the fairing of the data of figure 10.

For values of q_e less than 400 lb/sq ft, there was an increase in A_e with propeller rotational speed for constant blade angle as shown by data points of figure 10. The increase of A_e with rotational speed could not be attributed to any effects of blade resonance as A_e for the $\beta_{0.75R} = 30°$ conditions was obtained by directly using previously reported data of reference 3 for the same rotational speeds. It is believed that propeller operation changed the blockage and, hence, the 1xP excitation, as it was indicated that a partial stream blockage occurred with the wake-survey rakes in the positions shown in figure 4 as determined from the wind-tunnel calibrations discussed in reference 1.

Figure 10 shows that the effective airstream angles were small for all conditions, varying from about 1.0° at a rotational speed of 1,350 rpm to about 2.6° at 2,000 rpm. There was little effect of increasing the dynamic pressure except at 2,000 rpm where the extrapolated curve shows a decrease of about 0.5° over the range of dynamic pressure.

REFERENCES

1. Evans, Albert J., and Liner, George: A Wind-Tunnel Investigation of the Aerodynamic Characteristics of a Full-Scale Supersonic-Type Three-Blade Propeller at Mach Numbers to 0.96. NACA RM L53F01, 1953.

2. Wood, John H., and Swihart, John M.: The Effect of Blade-Section Camber on the Static Characteristics of Three NACA Propellers. NACA RM L51L28, 1952.

3. Gray, W. H., Hallissy, J. M., Jr., and Heath, A. R., Jr.: A Wind-Tunnel Investigation of the Effects of Thrust-Axis Inclination on Propeller First-Order Vibration. NACA RM L50D13, 1950.

4. Feigenbaum, David, and Comeau, R. E.: Calculation of Natural Fundamental Vibration Frequencies and Bending Moments on Several Variations of A39SFN-125 Propeller Blade Design. Rep. No. AB-713-W-1 (Contract No. P.O. 60609 AF 33 (038)-10583), Cornell Aero. Lab., Inc., Dec. 27, 1951.

5. Davidson, Anthony: Calculation of "1P" Propeller Resonance and First Mode Vibration Frequency. Memo. Rep. WCNB-580-19-2, Wright Air Dev. Center, U. S. Air Force, Oct. 15, 1951.

6. Rogers, Robert A.: Method for Determining 1xP Amplification. Eng. Rep. No. 609, Aeroproducts Div., General Motors Corp. (Dayton, Ohio), May 7, 1951.

7. Den Hartog, J. P.: Mechanical Vibrations. Second ed., McGraw-Hill Book Co., Inc., 1940, p. 62.

8. Gray, W. H., and Solomon, William: An Investigation of Propeller Vibrations Excited by Wing Wakes. NACA RM L51G13, 1952.

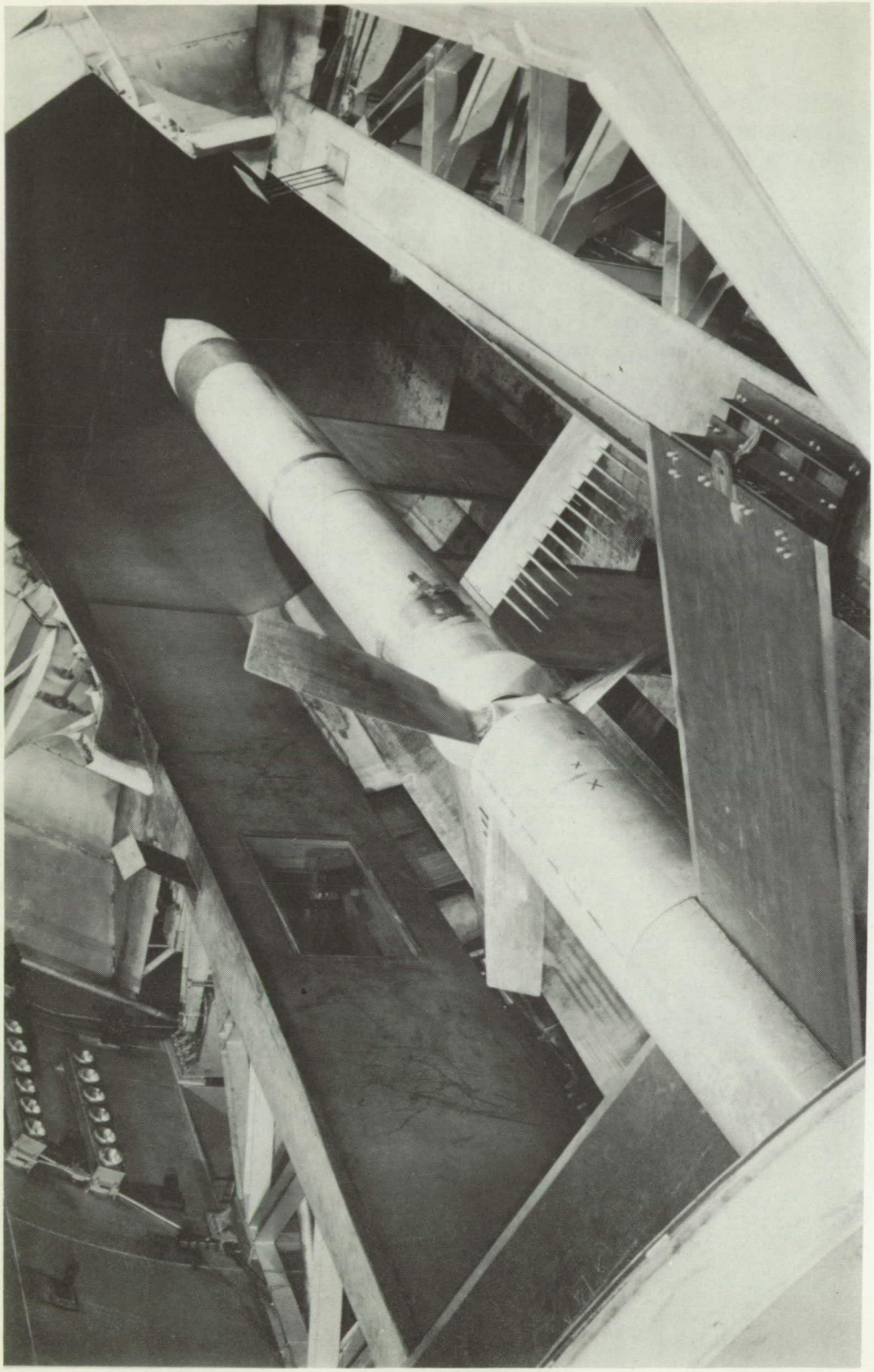

L-76249

Figure 1.- Aeroproducts A39SFN-161A propeller mounted on NACA 6,000-horsepower propeller dynamometer installed in Langley 16-foot transonic tunnel (looking downstream).

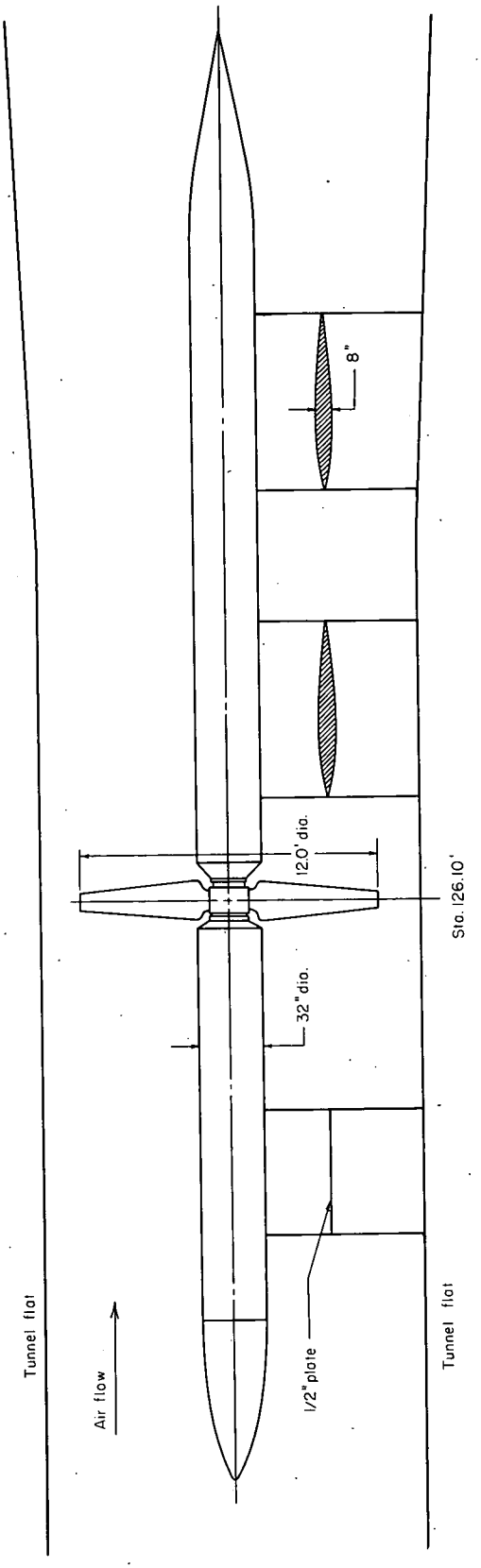

Figure 2.- Side view of dynamometer and cylindrical body installed in test section of Langley 16-foot transonic tunnel.

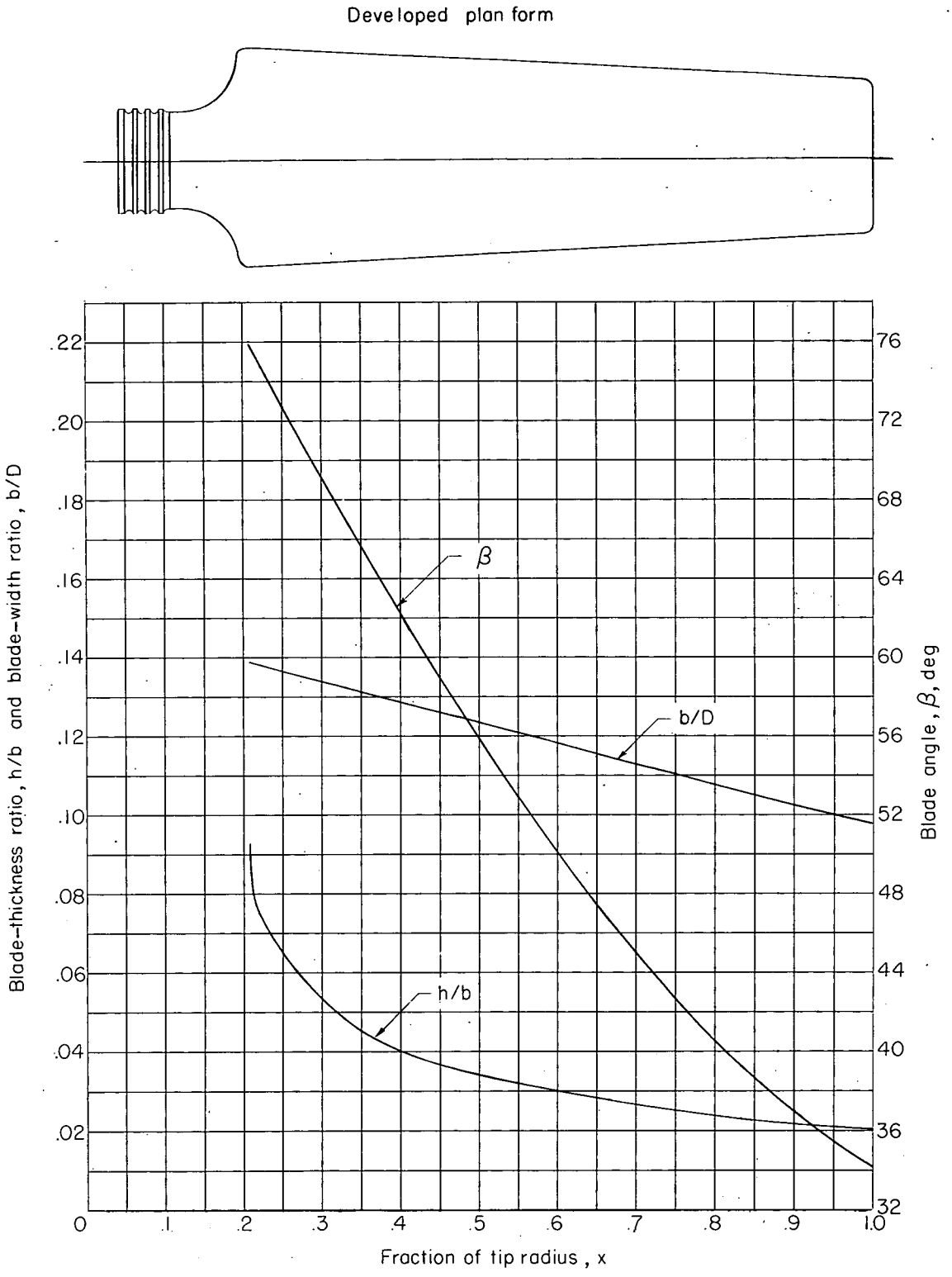

Figure 3.- Aeroproducts A91A1-144-0 propeller blade-form characteristics.

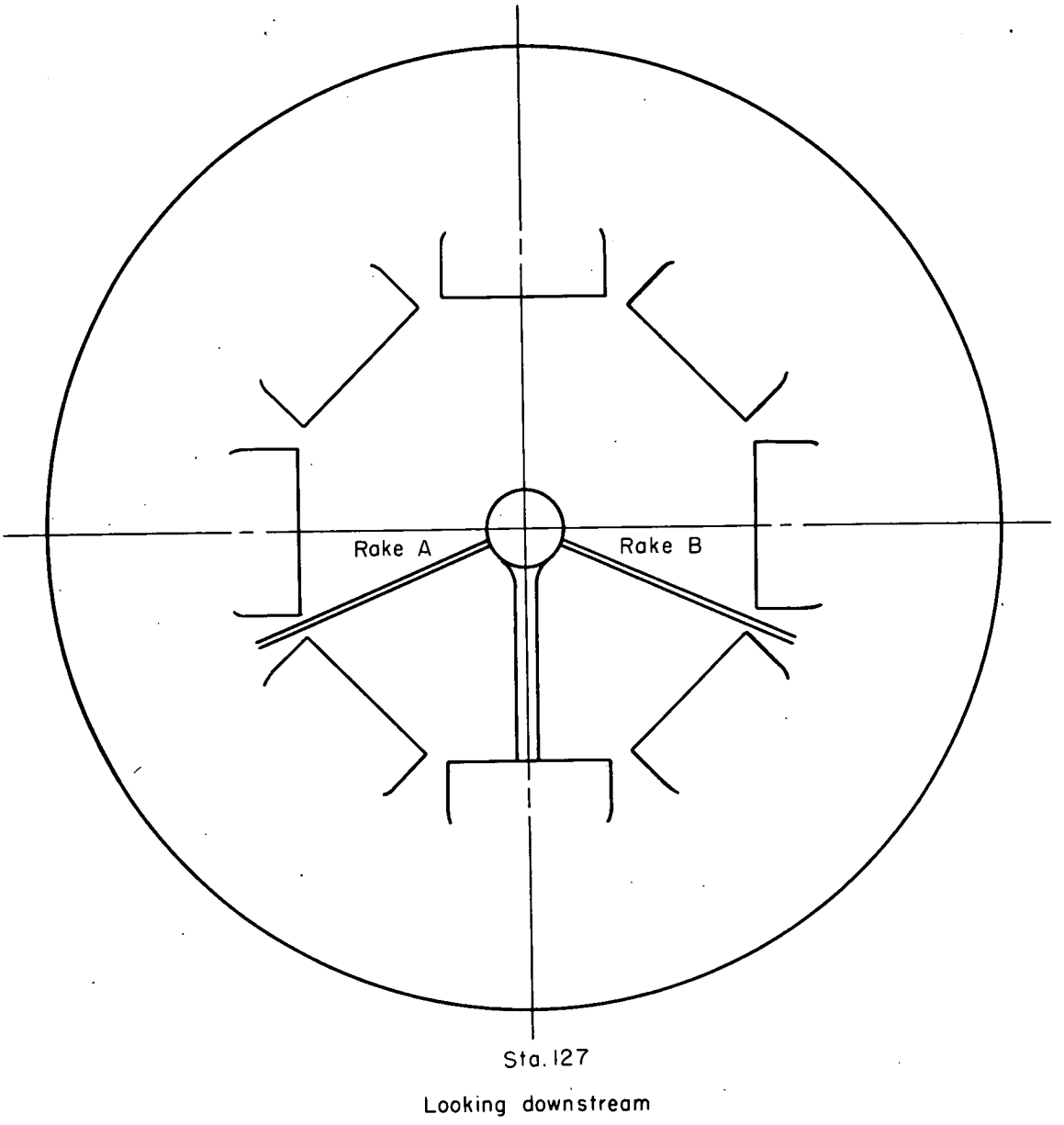

Figure 4.- Sectional view of tunnel showing dynamometer and survey rakes mounted in test section.

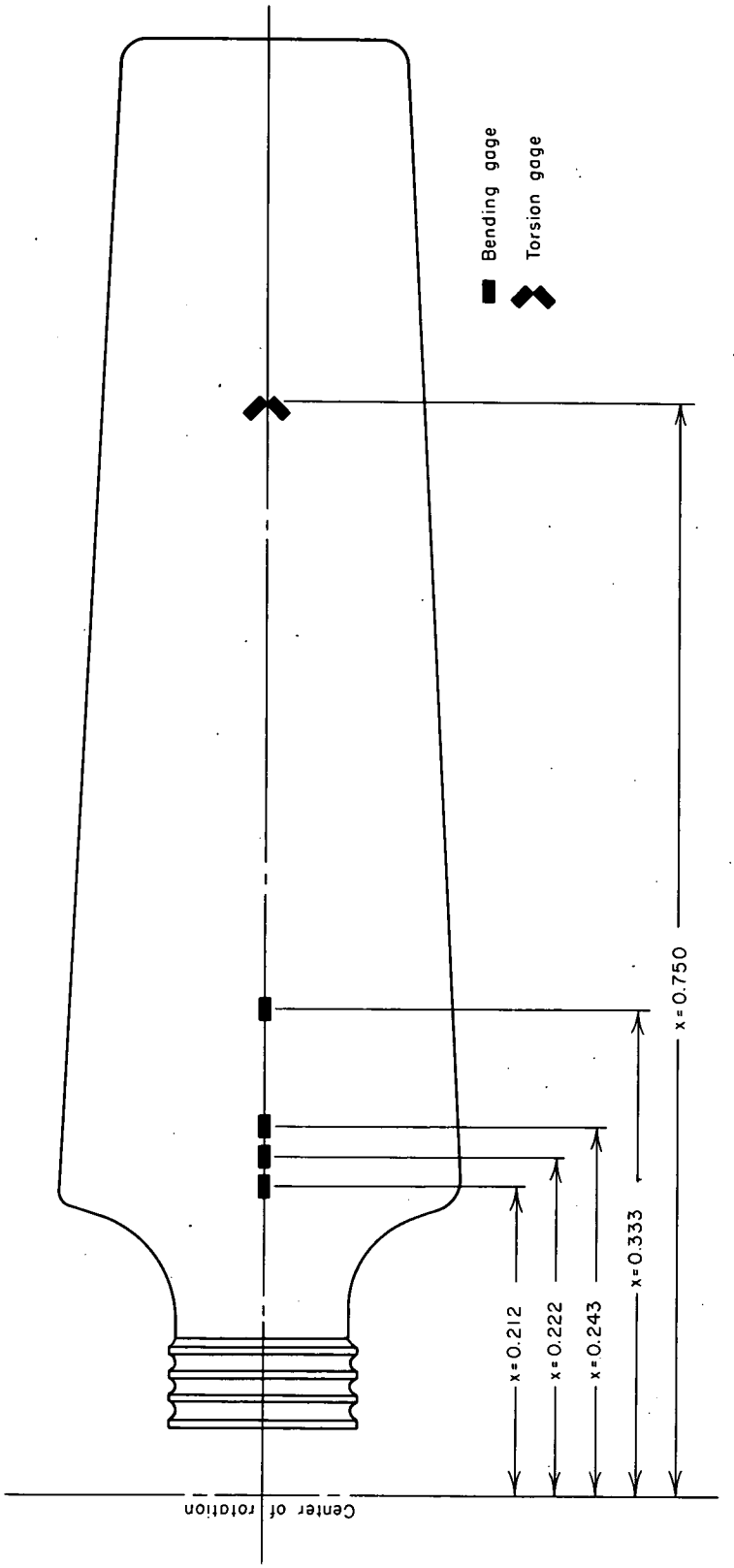

Figure 5.- Blade plan-form of Aeroproducts A91A1-144-0 propeller showing strain-gage locations.

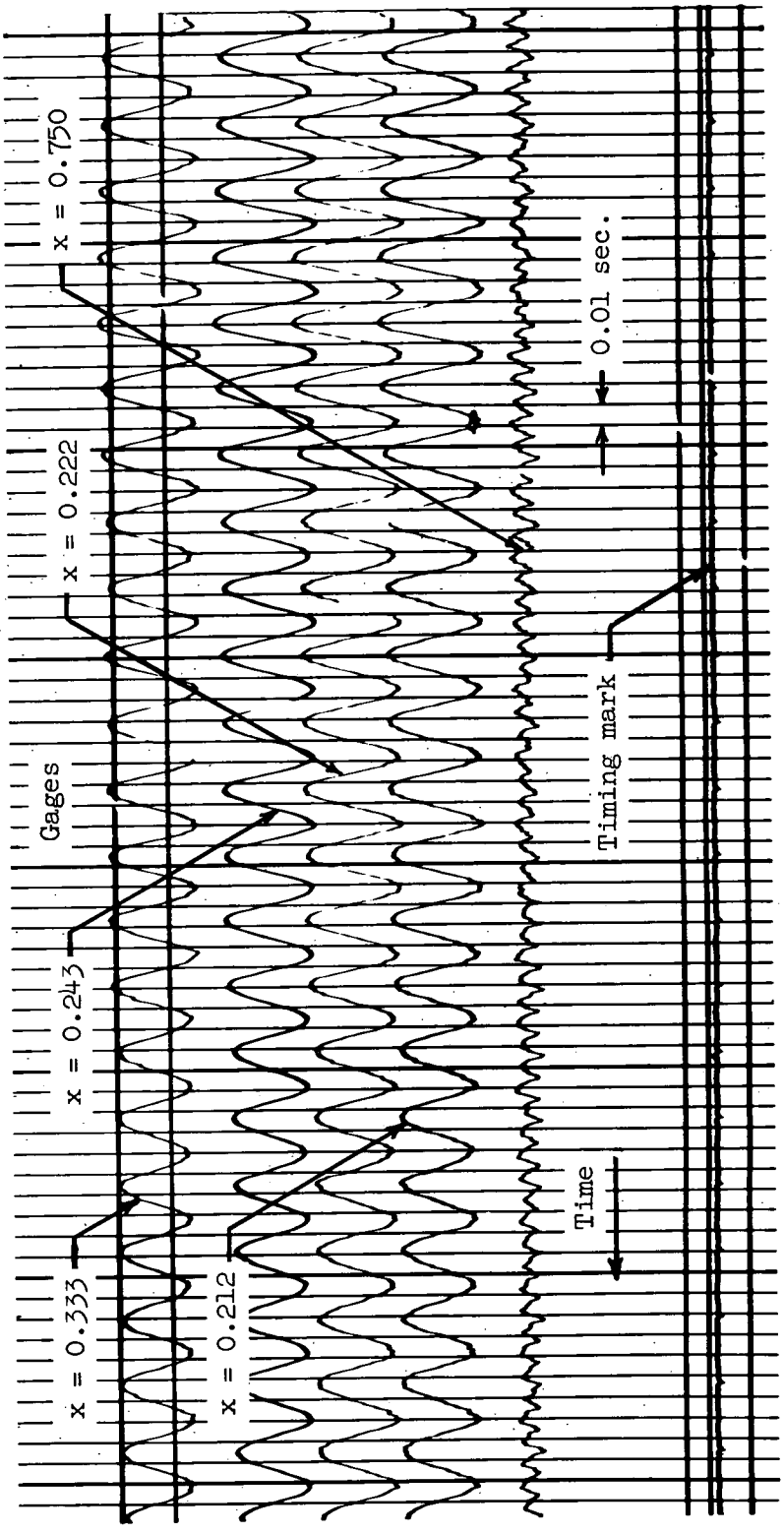

Figure 6.- Typical oscillograph record showing variation of lxP stress with time.

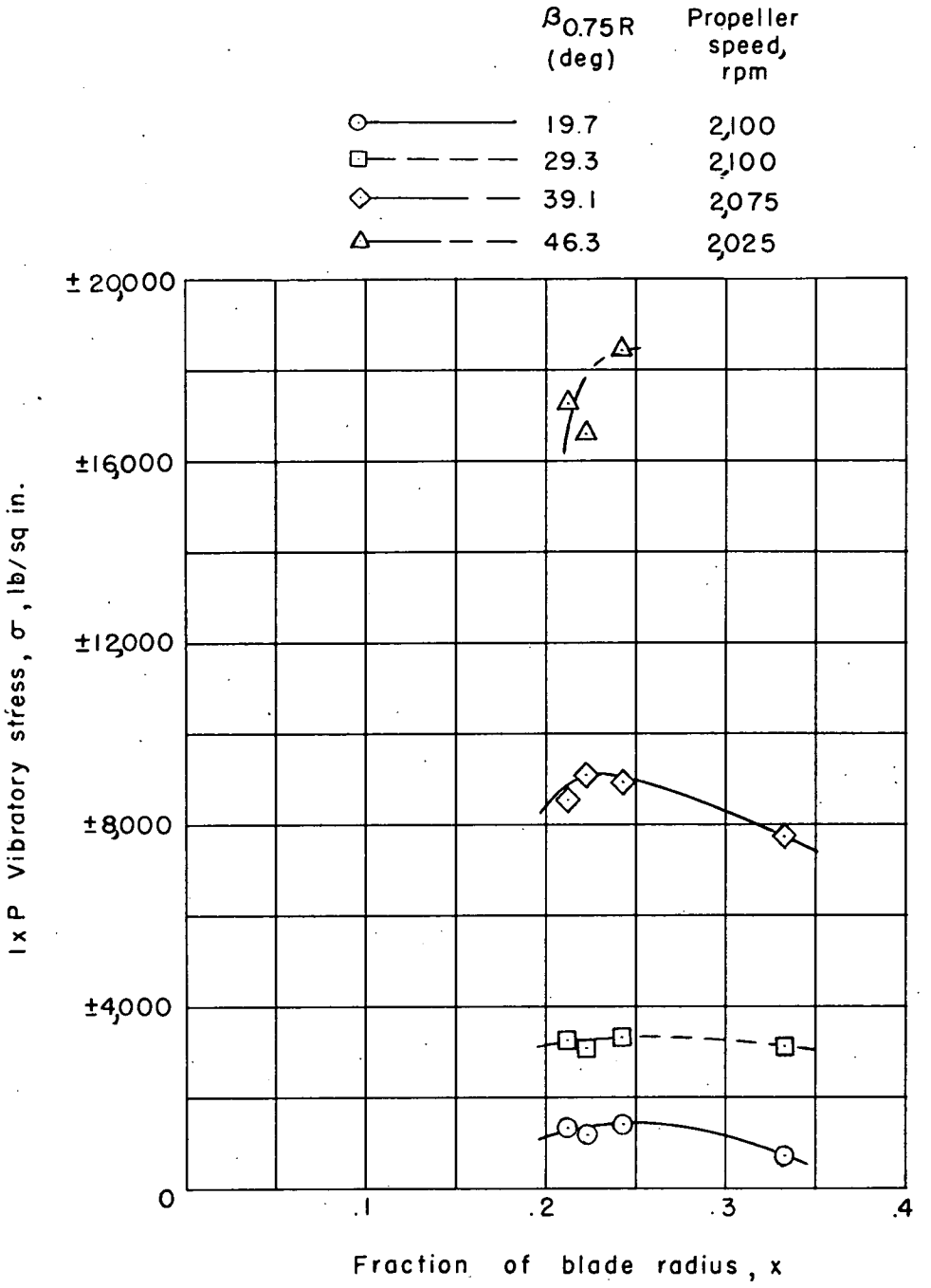

Figure 7.- Radial distribution of 1xP vibratory bending stresses.

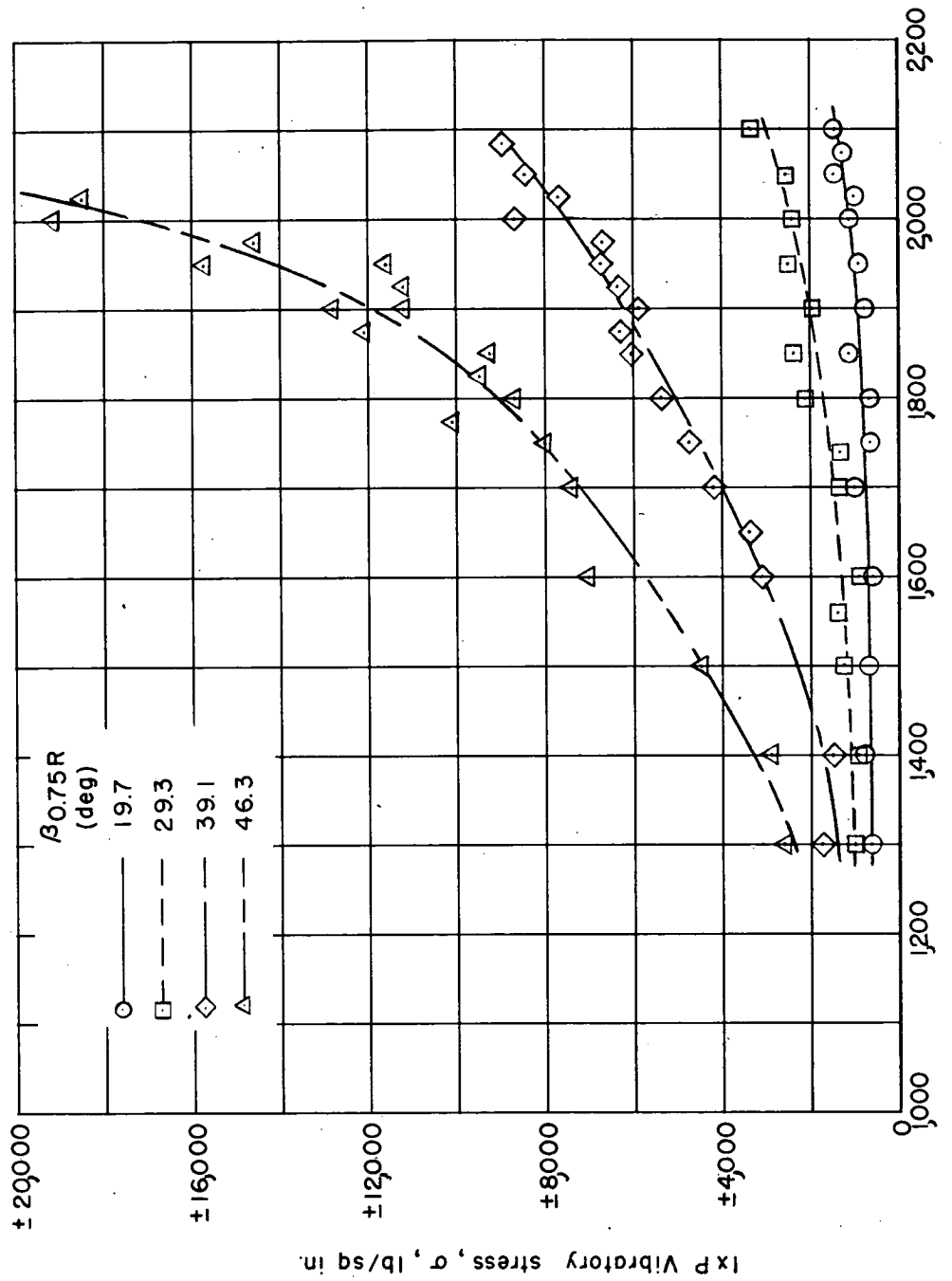

Figure 8.- Variation of 1xP vibratory stress, measured at x = 0.243 radius station, with rotational speed.

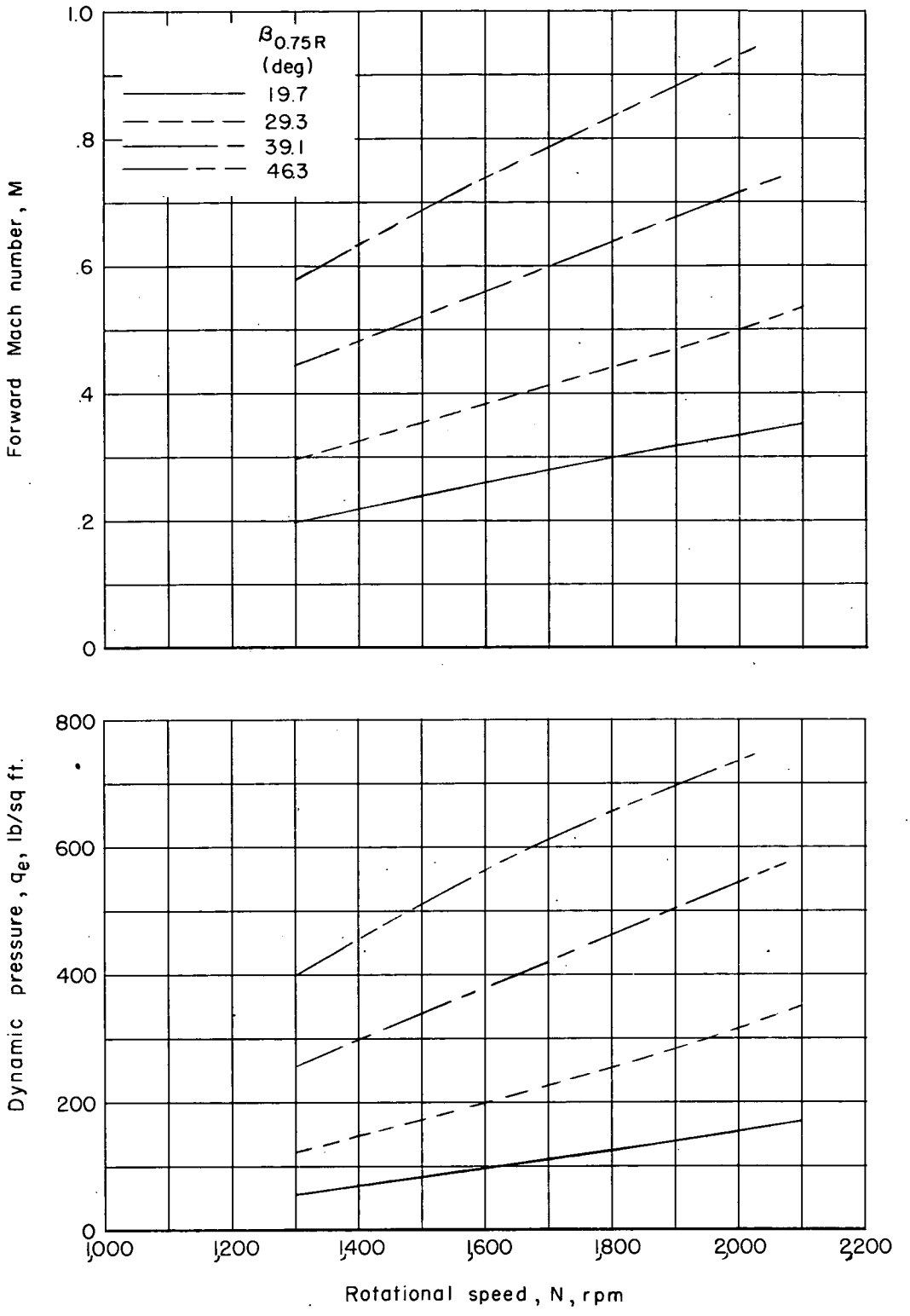

Figure 9.- Change in forward Mach number and dynamic pressure with blade angle for rotational-speed range investigated.

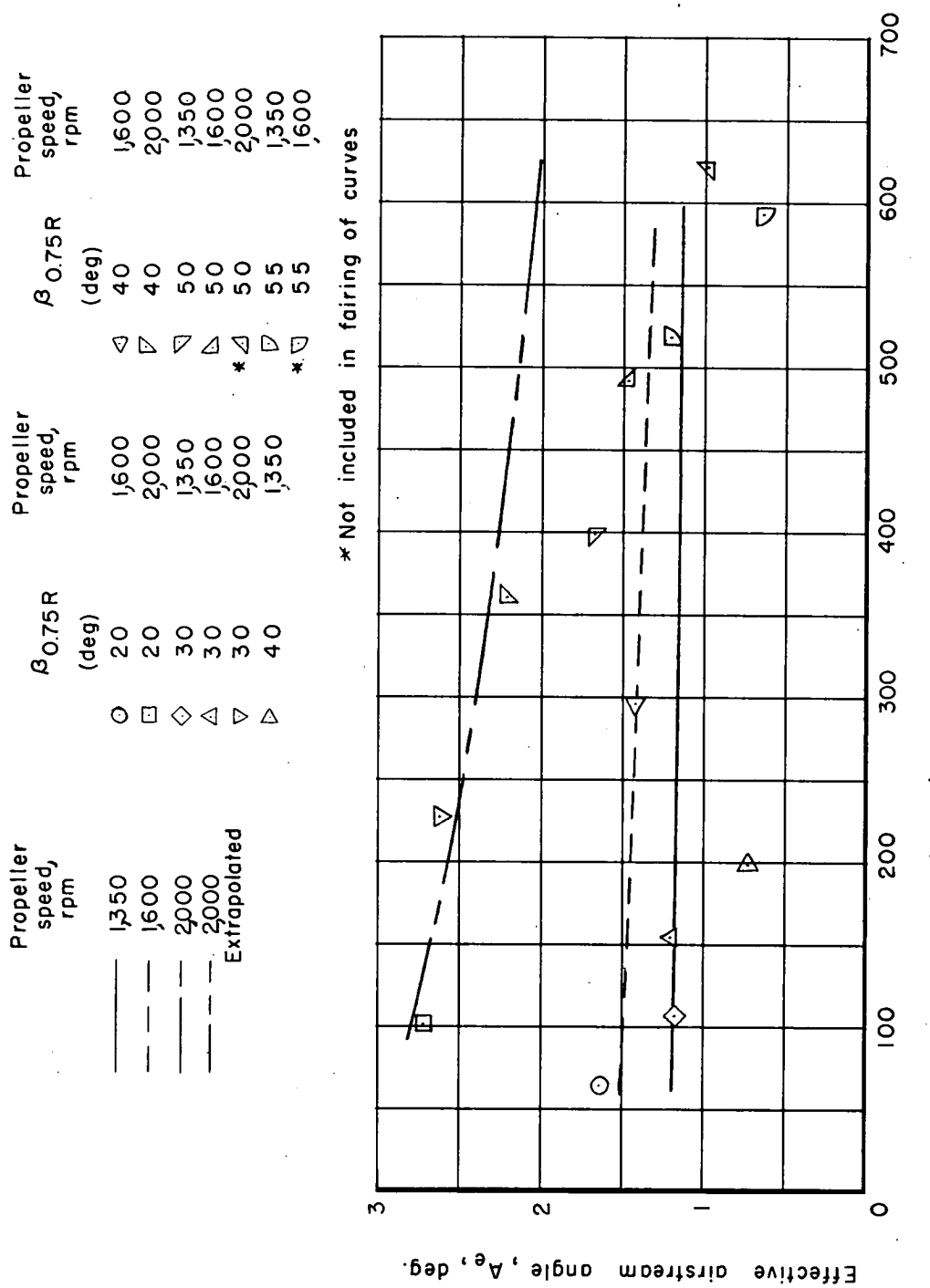

Figure 10.- Effective airstream angles A_e determined from 1xP vibratory-stress data obtained on NACA 10-(3)(08)-03 three-blade propeller.

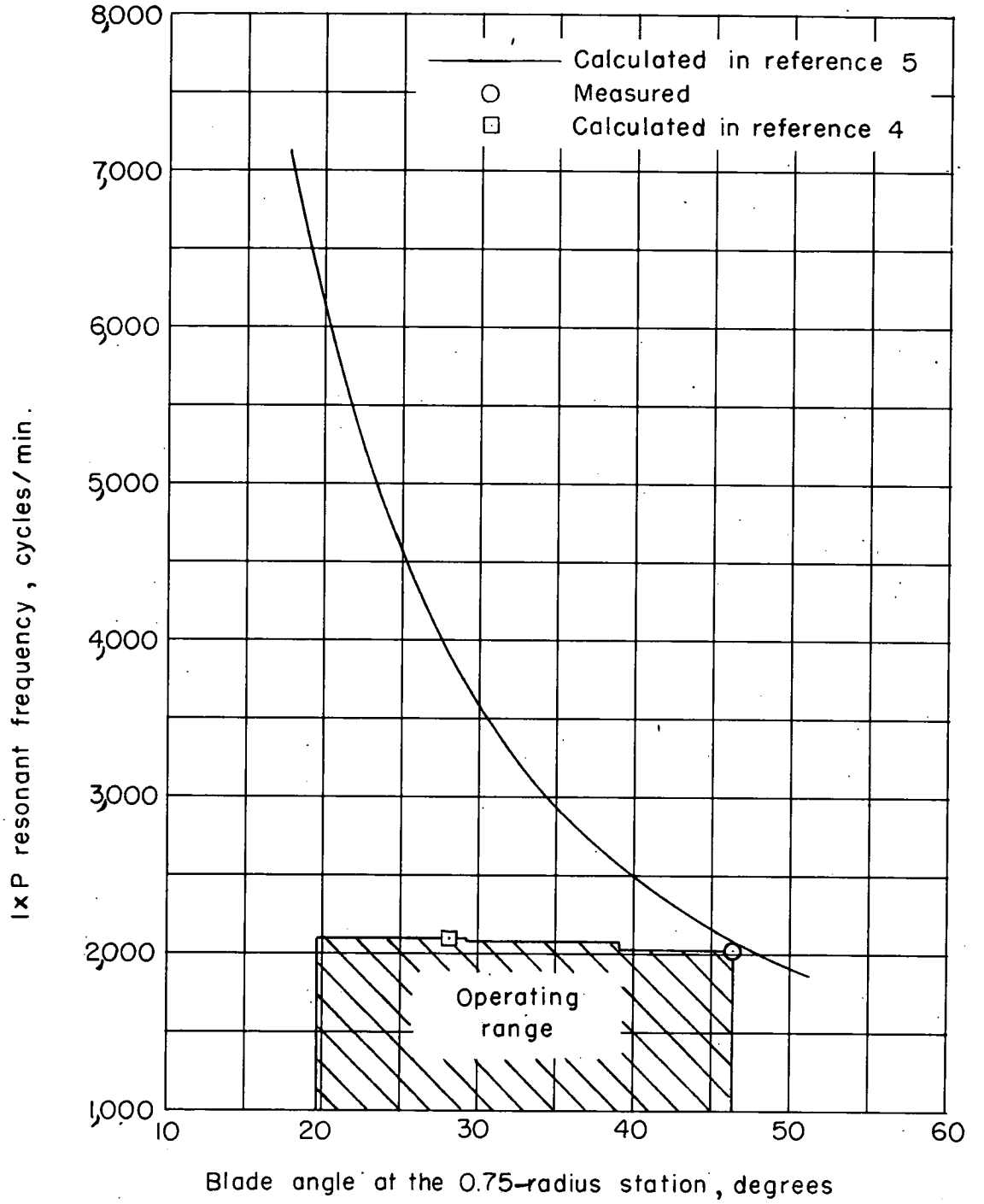

Figure 11.- Comparison of calculated 1xP resonant frequencies with measured apparent resonant frequency for Aeroproducts A39SFN-161A propeller.

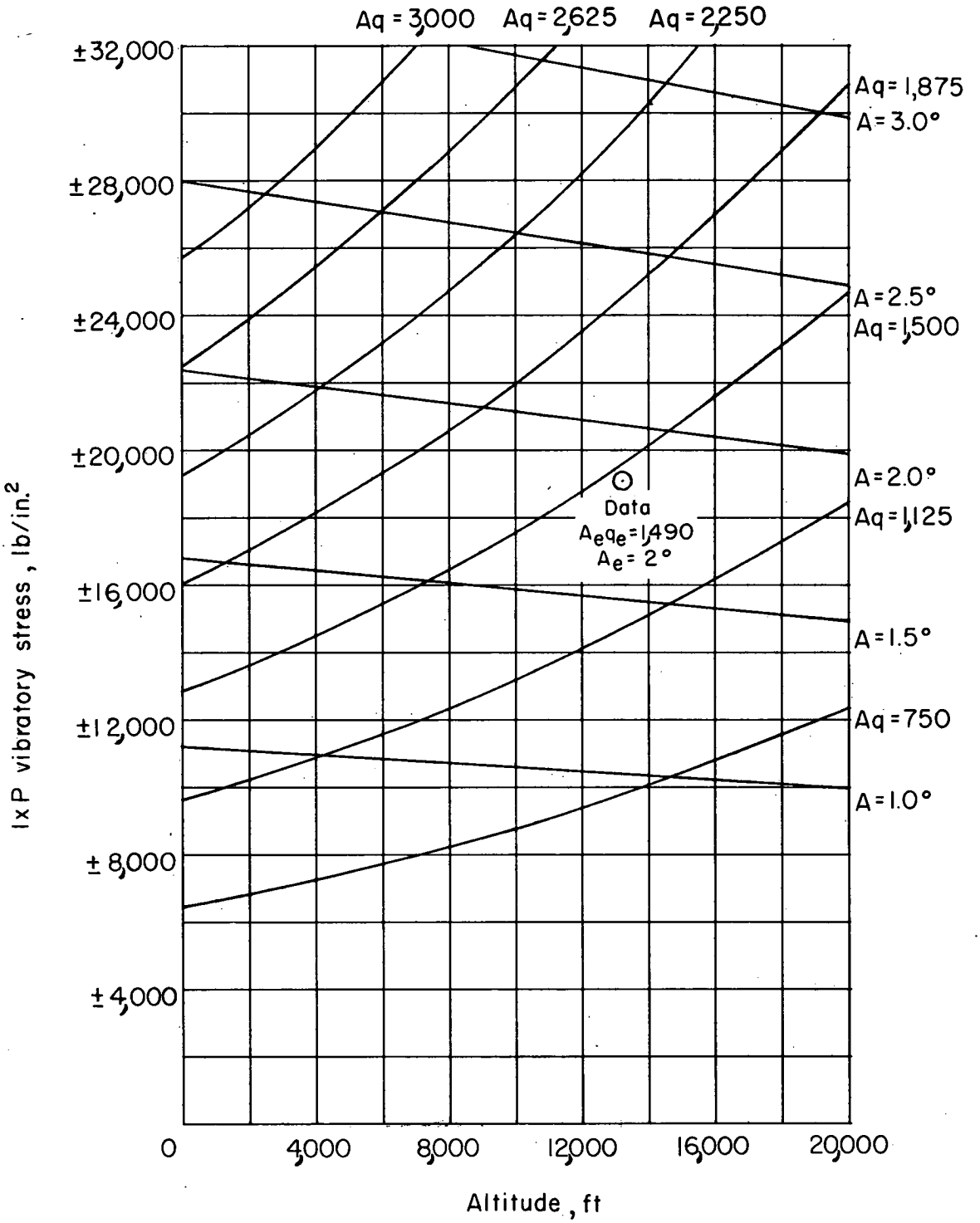

Figure 12.- Variation of apparent resonant 1xP vibratory stress with altitude for various thrust-axis inclination angles at M = 0.94, N = 2,025 rpm, $C_T \approx 0$, and $\beta_{0.75R} = 46.3°$.

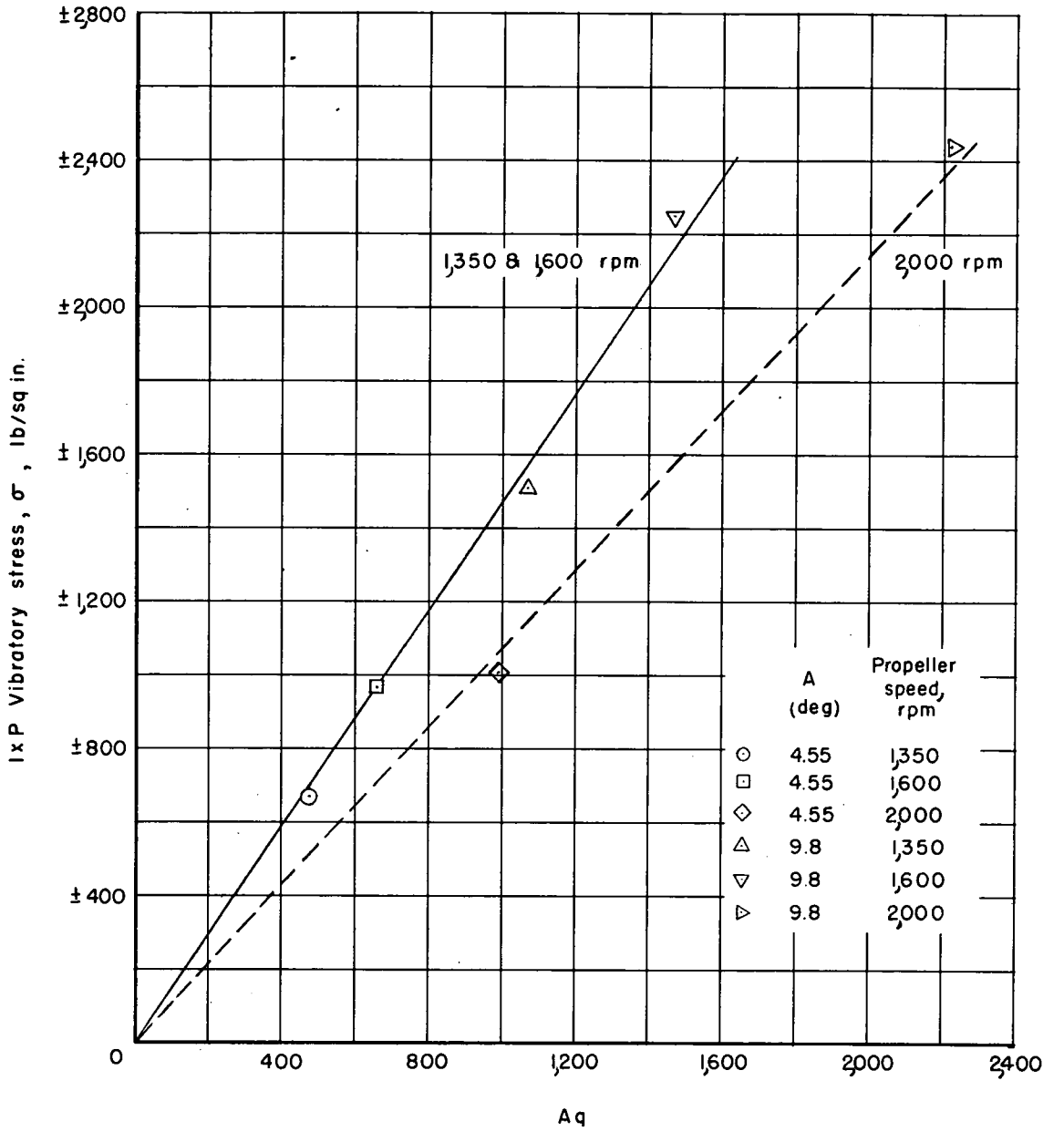

Figure 13.- Variation of 1xP vibratory stress, measured at x = 0.45 radius station, with Aq for NACA 10-(3)(08)-03 propeller operating at $C_T \approx 0$ and $\beta_{0.75R} = 30^\circ$. Data obtained during investigation reported in reference 3.

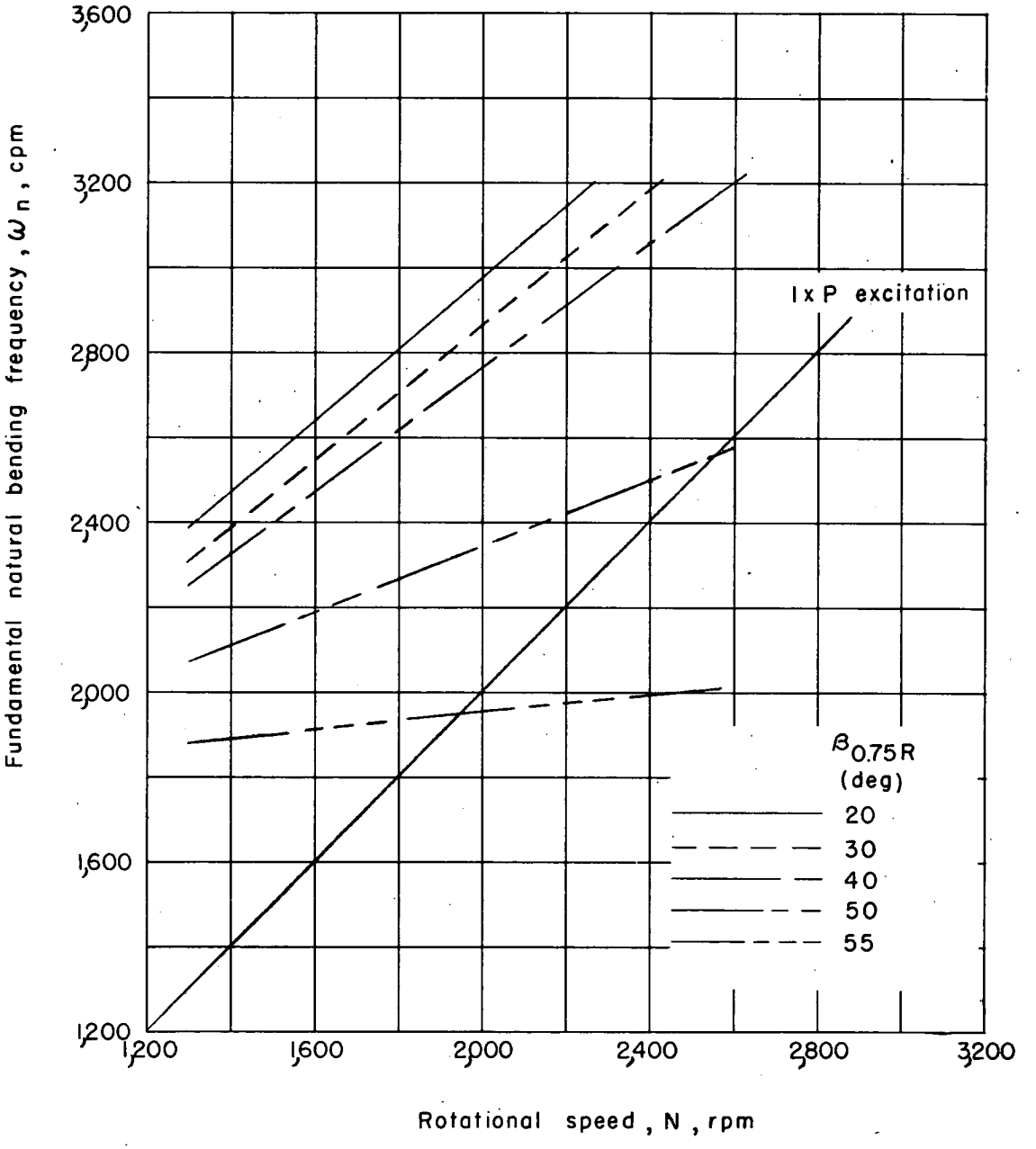

Figure 14.- Variation of fundamental natural bending frequency with rotational speed of NACA 10-(3)(08)-03 three-blade propeller as calculated by the Propeller Laboratory of the Wright Air Development Center.

NACA-Langley - 11-2-54 - 325